ACS APPLIED MATERIALS & INTERFACES

Research Article

www.acsami.org

Large-Area One-Step Assembly of Three-Dimensional Porous Metal Micro/Nanocages by Ethanol-Assisted Femtosecond Laser Irradiation for Enhanced Antireflection and Hydrophobicity

Guoqiang Li,[†] Jiawen Li,[†] Chenchu Zhang,[†] Yanlei Hu,*[,†] Xiaohong Li,[‡] Jiaru Chu,[†] Wenhao Huang,[†] and Dong Wu*[,†]

[†]Micro/Nano Engineering Laboratory, University of Science and Technology of China, Hefei, Anhui 230026, People's Republic of China

[‡]Extreme Conditions Material Properties Laboratory, Southwest University of Science and Technology, Mianyang, Sichuan 621010, People's Republic of China

Supporting Information

ABSTRACT: The capability to realize 2D−3D controllable metallic micro/nanostructures is of key importance for various fields such as plasmonics, electronics, bioscience, and chemistry due to unique properties such as electromagnetic field enhancement, catalysis, photoemission, and conductivity. However, most of the present techniques are limited to low-dimension (1D−2D), small area, or single function. Here we report the assembly of self-organized three-dimensional (3D) porous metal micro/nanocages arrays on nickel surface by ethanol-assisted femtosecond laser irradiation. The underlying formation mechanism was investigated by a series of femtosecond laser irradiation under exposure time from 5 to 30 ms. We also demonstrate the ability to control the size of micro/nanocage arrays from 0.8 to 2 μm by different laser pulse energy. This method features rapidness (~10 min), simplicity (one-step process), and ease of large-area (4 cm^2 or more) fabrication. The 3D cagelike micro/nanostructures exhibit not only improved antireflection from 80% to 7% but also enhanced hydrophobicity from 98.5° to 142° without surface modification. This simple technique for 3D large-area controllable metal microstructures will find great potential applications in optoelectronics, physics, and chemistry.

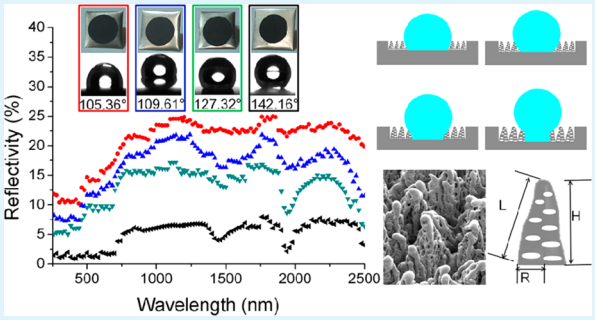

KEYWORDS: *femtosecond laser 3D processing, large-area, porous metal micro/nanocages arrays, antireflection, surface wettability*

1. INTRODUCTION

Metallic micro/nanostructures with controllable 2D−3D geometries have been attracting great attention due to their many promising applications ranging from plasmonics,[1,2] electronics,[3] and bioscience[4] to chemistry.[5,6] Significant effort has been devoted to the exploration of effective approaches for realizing various controllable metallic micro/nanostructures, investigating their performance, and exploring their novel applications. For example, conventional top-down microfabrication methods containing electron beam lithography,[7] focused ion beam (FIB),[8] and X-ray lithography[9] have been widely used in metal micro/nano structures fabrication due to their high resolution, but how to effectively and economically produce such nanostructures with large area is still a big challenge. On the other hand, bottom-up methods[10−13] by combining colloidal microsphere self-assembly, metal deposition and lift-off processing were usually used for fabricating 2D period metal microstructures. In addition, an advanced two-photon polymerization (TPP) technique[14,15] combined with a site-selective metal deposition technique has been developed for fabricating more complex structures with ~100 nm resolution, which are useful in some specific applications. However, the process is complicated, and the area is usually up to several hundred square micrometers. Moreover, many of them are limited for general use such as microelectronics, plamonics, and nanophotonics due to the nonconducting polymeric structures. Thus, it is highly desirable to develop a convenient technology that is able to rapidly fabricate large-area 2D−3D micro-nanostructured metallic surfaces with excellent performance.

Recent studies have shown that self-organized metallic micro/nanostructures can be created on metal surfaces using femtosecond laser direct irradiation. Among these structures, the most common ones are the subwavelength ripples,[16,17] nanotextured conical microstructures,[18] jetlike structure,[19] which can greatly improve the optical, biological, and chemical properties of metallic material surface, such as color display,[20−24] anticounterfeiting[22,24] and optical data storage.[24] Nevertheless, these structures are mostly limited to one-

Received: September 17, 2014
Accepted: December 4, 2014
Published: December 4, 2014

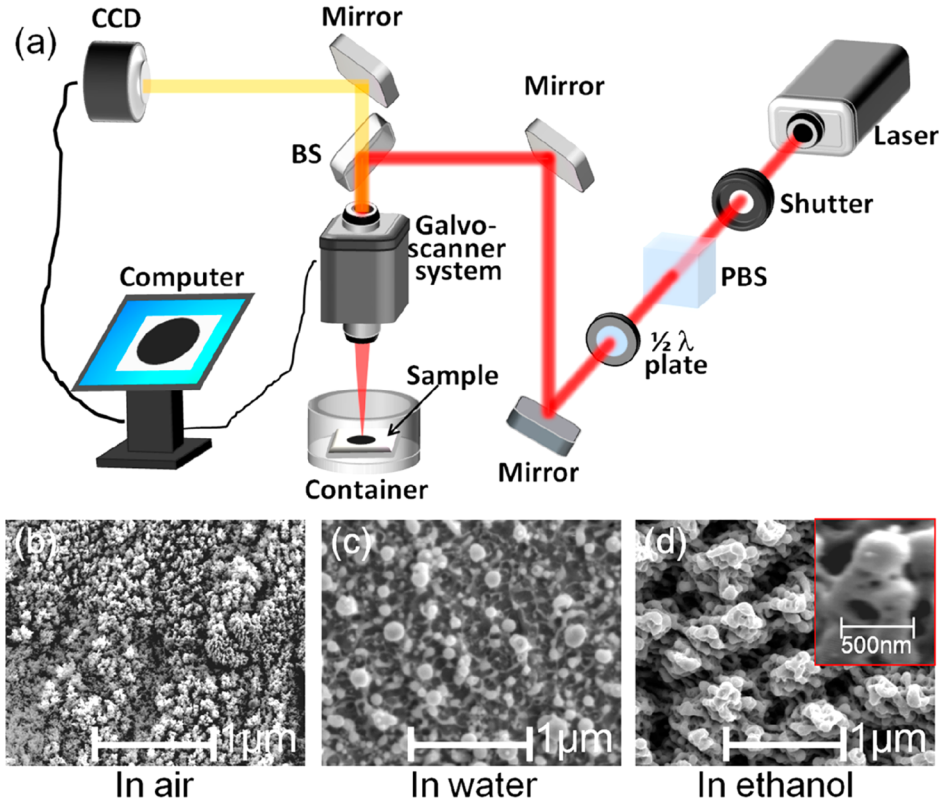

Figure 1. Large-area one-step assembly of 3D micro/nanocage-like structures by ethanol-assisted femtosecond laser irradiation. (a) Experimental setup for fabricating micro/nanocage-like structures. (b) SEM image of the nickel surface irradiated in air. The laser-induced microstructures are irregular. (c) Spherical microstructures formed by laser irradiation in distilled water. (d) Unique 3D micro/nanocage-like structures fabricated in ethanol solvent. The inset is 45° tilted SEM image of single micro/nanocage-like microstructures. The size of micro/nanocage is ~0.8 μm, and the average size of its surface nanohole is ~10−100 nm.

dimensional (1D) or two-dimensional (2D) features, which seriously limit their multifunctionality. As a kind of important ferromagnetic metal, nickel shows outstanding optical, catalytic, electrical, and superior resistant characteristics to corrosion, which makes it widely applicable in electronics,[25] nickel-batteries,[26] alloy,[27] and chemical catalyst.[28,29] Although some functional 1D−2D structures such as ripples,[30,31] mounds,[32−34] and cones[32−34] have been formed on nickel surfaces, there are still few reports on the controllable fabrication of complex 2D−3D micro/nanostructures and systemic investigation of their multifunctions.

Here, we report a facile and rapid method to fabricate large-area (4 cm^2 or more) three-dimensional (3D) porous metal micro/nanocages arrays with 0.8 μm sizes by one-step ethanol-assisted femtosecond laser irradiation on nickel surfaces. The underlying formation mechanism was investigated by a series of femtosecond laser irradiation under exposure time from 5 to 30 ms. By controlling the laser energy, micro/nanocage arrays with different sizes from 0.8 to 2 μm were obtained. Furthermore, these porous micro/nanocages arrays exhibit multiple functions, which can endow the nickel surfaces with not only low reflectivity over a broad wavelength range but also improved hydrophobic ability.

2. EXPERIMENTAL SECTION

To fabricate micro/nanocage-like structures, a regenerative amplified Ti:sapphire femtosecond laser system (Legend Elite-1K-HE, Coherent, America) that generates 104 fs pulses at the repetition rate of 1 kHz with a central wavelength of 800 nm is employed for irradiation. The schematic fabrication process is shown in Figure 1a. In our experiment, the mechanically polished nickel plates (Chinese New Metal Materials Technology Co., Ltd., China) with purity of 99.99% and dimension of 0.5 × 20 × 20 mm^3 are chosen as targets. The nickel plate is stuck to the bottom of a 20 mL container (Petri dish), which is filled with ethanol (purity of 99.3%). The linearly polarized laser beam is guided normally onto the nickel surface through the ethanol layer by a galvo-scanner system (SCANLAB, Germany) equipped with a 63 mm telecentric $f\theta$ lens. This lens can enhance laser scanning systems by providing a focused laser beam perpendicular to the process surface and thus eliminate inconsistencies associated with nonflat surfaces. The diameter of the focused spot is approximately 30 μm. The pulse energy was adjusted with a variable attenuator that consisted of a half-wave plate and a low dispersion polarizer. The exposure time of the laser beam on the sample surfaces is controlled by a computer-controlled high-speed shutter. To prepare porous micro/nanocages, the experimental conditions were precisely controlled and optimized. The incident laser pulse energies are set from 0.05 to 0.20 mJ/pulse. The step size between the adjacent scanning lines is 50 μm, and the total scanning time is ~10 min. During the fabrication process, the CCD camera was connected to computer for clear online observation in nickel pattern surface. In contrast, the nickel plates are also stuck to the bottom of the empty Petri dish, or it is filled with distilled water for laser irradiation with the same parameters as in ethanol. After laser processing, the structural properties of the samples were observed by scanning electron microscope (SEM, JSM-6700F, JEOL, Tokyo, Japan). To quantitatively characterize the spectral responsivity, the wavelength dependence of total reflectance in the UV, visible, and IR regions (250−2500 nm) was measured by a spectrophotometer (SOLID3700, Shimadzu, Japan) with an integrating sphere, which can effectively collect the stray lights by the diffuse reflections. The photographs of the polished and processed nickel were taken by a digital camera (PowerShot SX600HS, Cannon, Japan). The wettability was investigated by dripping a 4 μL water droplet on the processed

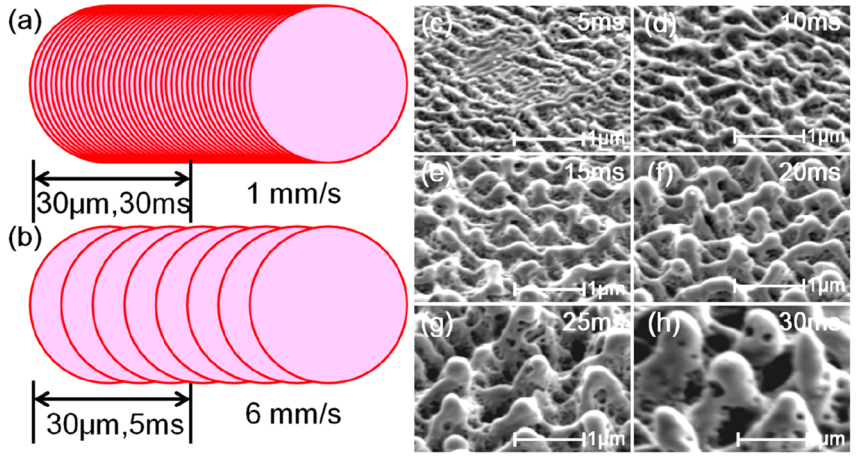

Figure 2. The in situ evolution process of the 3D micro/nanocage-like structures investigated by different irradiation time. (a) and (b) The schematic diagram for scanning speed of 1 and 6 mm/s, respectively. (c–h) 45° tilted SEM images of the morphology of nickel surface structures irradiated with different exposure time from 5 to 30 ms.

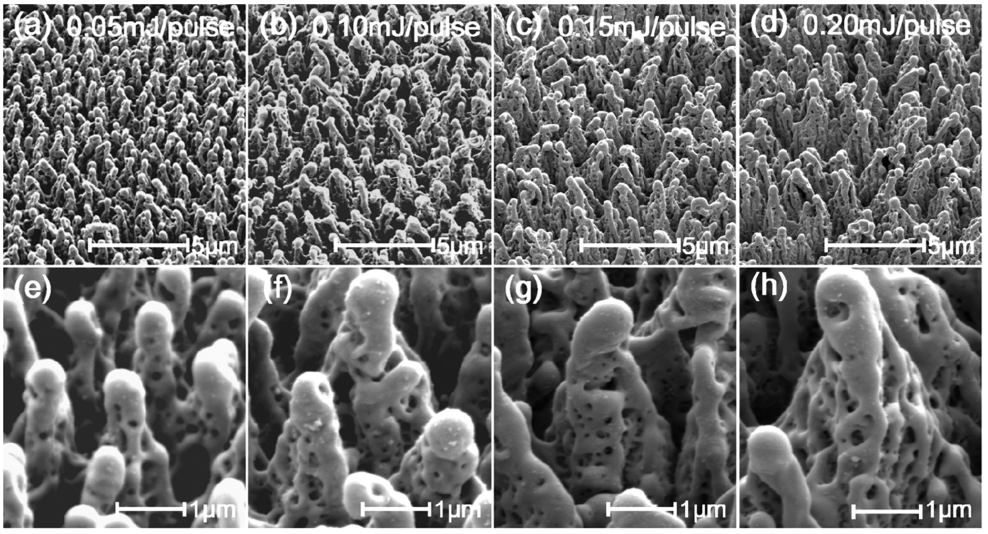

Figure 3. Precisely controlling the micro/nanocages size by adjusting the laser pulse energy. (a–d) SEM images of various 3D micro/nanocages arrays produced at pulse energy of 0.05, 0.10, 0.15, and 0.20 mJ/pulse, respectively. The scanning speed is 1 mm/s. (e–h) Magnified SEM images of micro/nanocages arrays with various sizes (0.82, 1.12, 1.54, and 1.91 μm).

nickel surfaces to perform the contact angle (CA) measurements with contact-angle goniometer (CA100C, Innuo, Shanghai, China) by a sessile drop method.[48] The average CA values were obtained by measuring the same samples in three different positions. The digital drop image taken by the digital camera was processed by the software (CA100C, Innuo, Shanghai, China) automatically, which can calculate the contact angles from the drop shape.

3. RESULTS AND DISCUSSION

3.1. Large-Area One-Step Formation of 3D Micro/Nanocage-like Structures by Ethanol-Assisted Femtosecond Laser Irradiation. From Figure 1b–d, it is clearly indicated that different microstructures are formed on the femtosecond laser radiated surface of nickel under different ambient environments. The laser energy is the same, ~0.05 mJ/pulse. We found that the formed structures in air and in water are 2D with 0.02–0.3 μm and 0.03–0.4 μm size, while the ones in ethanol look like 3D micro/nanocage with 0.8 μm size. The comparison of air, distilled water, and ethanol ambient environments clearly indicates the unique 3D micro/nanocage-like structures can only be formed in ethanol [Supporting Information, Figure S1]. The formation of the micro/nanocage arrays by ethanol-assisted femtosecond laser irradiation raises a fundamental question: how are the structures induced? Compared to the irradiation in gaseous environment, the formation process in ethanol is more complex due to the effect by laser-induced plasma of the ambient liquid, enhanced heat conduction, intensified acoustic pressure, increased shock wave, and explosive vaporization.[35−37] The formation of unique structures may be caused by the competition of several processes since the phase transition occurs both in the solid and adjacent liquid.[37] Femtosecond laser may produce the superheated substance and a transient zone of elevated pressure near the target, which brings the surrounding liquid to a supercritical state.[35] As a result, the pressure wave interacts with the melt layer on the target surface, and its morphology is perturbed.[37] This surface profile is frozen upon cooling by the subsequent liquid to prevent being smeared by the surface tension of the melt.[37−39]

3.2. The in Situ Evolution Process of the 3D Micro/Nanocage-like Structures Investigated by Different

dx.doi.org/10.1021/am506291f | ACS Appl. Mater. Interfaces 2015, 7, 383−390

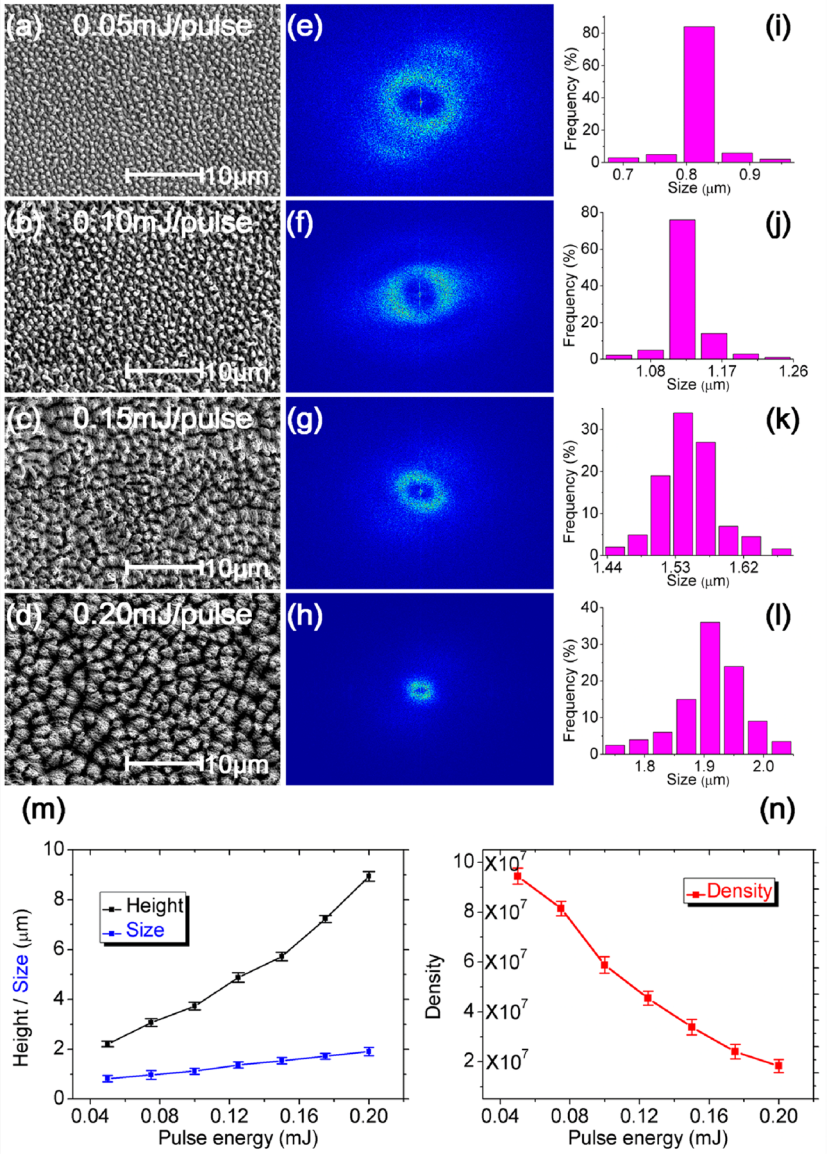

Figure 4. Quantitative analysis of the size distribution of various micro/nanocages. (a–d) Top view SEM images of the micro/nanocages produced at 0.05, 0.10, 0.15, and 0.20 mJ/pulse, respectively. (e–h) The 2D fast Fourier transformation (2D-FFT) results for the SEM images. (i–l) The typical size distribution histograms of the micro/nanocages based on the statistical calculations of all the SEM images. (m) The height and the size of the micro/nanocages as a function of the pulse energy. (n) The density of the micro/nanocages with different pulse energy.

Irradiation Time. The scanning of laser beam across the nickel surface ensures the uniform distribution of laser irradiation along the scanning line. The morphology of micro/nanocages depends strongly on the pulse energy and the irradiation time. In our experiment, the micro/nanocages arrays can be fabricated at scanning speed of 1 mm/s, even with the low pulse energy of 0.05 mJ/pulse. Therefore, the average irradiation time on the excitation spot is 30 ms, as shown in Figure 2a. To study the formation and evolution of the micro/nanocages, the scanning speed was set as 6 mm/s, and the average irradiation time on the excitation spot is 5 ms, as shown in Figure 2b. Then, the processing area was scanned for different times from 1 to 6, and the corresponding irradiation time on the excitation spot was 5, 10, 15, 20, 25, and 30 ms, respectively. After each radiation, the morphology was observed by SEM images, as shown in Figure 2c–h. Through this method, the formation mechanism was systemically investigated.

The evolution with increasing irradiation time reveals a clear formation process for the micro/nanocage-like structures. First, the laser induces plasma plume on the ethanol/nickel interface and ablates the nickel surface to form initial roughness, as shown in Figure 2c. Then, with the increasing irradiation time from 10 to 30 ms, the confined laser-induced plasma by ethanol[35,38] can further interact with the formed structures, which results in the growing structures [Figure 2d–h]. Because of the confinement of the pure ethanol, the laser-induced plasma can be pushed to a state of high temperature, high pressure, and high density.[35−39] Finally, the porous metal structures are formed. Additionally, the cooling effect of the confined ethanol on the laser-induced plasma also enhances the formation of the porous microstructures.[36−39]

3.3. Precisely Controlling the Micro/Nanocages Size by Adjusting the Laser Pulse Energy. On the basis of the evolution results, we also demonstrate the growth control of the micro/nanocage-like structures by adjusting the pulse

dx.doi.org/10.1021/am506291f | ACS Appl. Mater. Interfaces 2015, 7, 383−390

energy. Figure 3a–d indicates various porous micro/nanocage-like structures prepared under pulse energy ranging from 0.05 to 0.20 mJ/pulse at the scanning speed of 1 mm/s. From the magnified SEM images in Figure 3e–h, it can be seen that the height, size, and spacing of micro/nanocages depends on the pulse energy. As the pulse energy increases, the micro/nanocages become larger due to the stronger interaction of laser with nickel surfaces. At low pulse energy of 0.05 mJ/pusle, the laser can only induce micro/nanocage with size as small as 0.8 μm. With the increase of pulse energy, the laser-induced plasma is further expanded to produce a shock wave, higher temperature, and higher pressure at the nickel surface, so the higher and larger size of micro/nanocages are produced.

Judging from the SEM images, it is found that the distribution of these micro/nanocages is uniform and exhibit periodic. To further investigate the distribution of the micro/nanocages, the top-view SEM images of Figure 4a–d are subjected to a two-dimensional fast Fourier transformation (2D-FFT)[40,41] [Supporting Information, Figure S3], as shown in Figure 4e–h, which reveals that frequency spectrum is distributed into ring, and the radius of the ring is diffuse within a small range. This demonstrates that the micro/nanocages are formed with characteristic periodic distribution in all directions. Furthermore, the radius of the ring can reflect the denseness of the distribution. This can be confirmed from Figure 4e–h, from which we can see that the diameters of the rings are becoming smaller and smaller. The larger the diameter, the more intensive the micro/nanocages. Figure 4i–l shows typical size distribution histograms of the micro/nanocages, which are based on the statistical calculations of all SEM analysis. From Figure 4i,j, we can see that the sizes from 0.79 to 0.84 μm and from 1.09 to 1.13 μm almost occupy 80% of the micro/nanocages, respectively. Although the distributions are slightly in disorder, the frequency of the sizes from 1.50 to 1.58 μm and from 1.86 to 1.97 μm is also more than 80% [Figure 4k,l]. Generally, the sizes of the micro/nanocages are still uniform, and the average size increases with the increased pulse energy. Finally, from the statistical results in Figure 4m,n, it is revealed that the heights of the micro/nanocages increased, while the density (the number of the micro/nanocages per square centimeter) decreased with the increasing pulse energy. What's more, plenty of tiny nanoholes with the size from tens to hundreds of nanometers are formed over the entire micro/nanocage. To the best of our knowledge, the 3D multiscale porous micro/nanostructures prepared on nickel have not been reported. Our proposed method also shows the ability to control the size of the micro/nanocages by adjusting the laser energy.

3.4. Enhanced Antireflection and Hydrophobicity of Microstructured Nickel Surfaces under Different Laser Pulse Energy Irradiation. The processed nickel surfaces show black color, as shown in the digital photographs of Figure 5b, so the nickel surfaces' reflectance before and after femtosecond laser irradiation is also measured [Figure 5a]. It is evident that the reflectance of the black nickel surface is much lower than that of the polished one (~80%) over the entire wavelength range (0.25–2.5 μm). Furthermore, the reflection of structured nickel surfaces depends upon the height and spacing of the micro/nanocages. The larger the micro/nanocages, the lower the light reflection. Note that the black nickel produced with the pulse energy of 0.20 mJ/pulse only has less than 7% reflection in the entire wavelength range. This novel phenomenon is presumed to be related to the tapered morphology of the micro/nanocage and surface plasmon

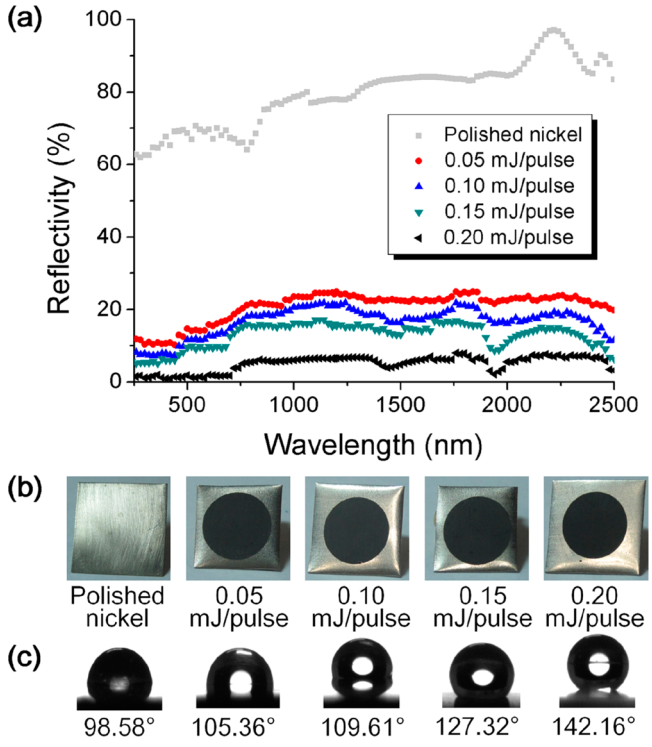

Figure 5. Enhanced antireflection and hydrophobicity of the microstructured nickel surfaces irradiated with different pulse energy. (a) Wavelength-dependent reflectance of polished and black nickel. The average reflectivity of the polished nickel is ~80%, while the one of the sample under 0.2 mJ/pulse is only 7%. (b) Photograph of the polished and black nickel. (c) The corresponding CA of the polished and black nickel without any low surface energy modification. Under the laser irradiation, the CA of the microstructured nickel is significantly increased 142.16°, much bigger than 98.58° for flat surface.

excitation. First, the tapered micro/nanocages can form effective graded refractive index layer at the air/solid interface[42–44] and significantly reduce the reflection. Second, the porous structures may form photonic traps and enable the incident light to be confined. Third, it was found that the lateral of the micro/nanocages with larger sizes were covered with many smaller-size nanoparticles and nanoholes. So, the incident light was effectively absorbed and multiply reflected by these nanoparticles and nanoholes due to surface-plasmon absorption. Finally, successive multiple reflection may take place between/inside the micro/nanocages, which further enhance the surface-plasmon absorption effect.[45] All these factors led to the lower reflection over a wide wavelength of 250–2500 nm.[19,43–45] The angle-dependent reflectance, for example, the micro/nanocages with size of 1.91 μm, was also investigated with incident angle of 6° and 12° [Supporting Information, Figure S4]. The measurements demonstrate that the angle has little impact on the reflectance. Although the reflectance from 1250 nm is higher than that of the normal-incidence reflection, it is still less than 10% in the range from 250 to 1250 nm. Moreover, the micro/nanocages are conductive due to the nickel substrate, so the electrical properties of these structures are very useful in optoelectronics, electronics, industry, and batteries.

It has been reported that the laser-machined micro/nanostructures have the ability to tune surface wettability, making the metal surface more hydrophilic or hydro-

dx.doi.org/10.1021/am506291f | ACS Appl. Mater. Interfaces 2015, 7, 383–390

phobic.[46−48] To investigate the wettability, the CA measurements on the processed nickel surfaces were performed. The wettability of the polished nickel is also measured for comparison. The nickel with clean surfaces is initially hydrophilic;[49,50] however, the polished nickel in our case shows hydrophobic [Figure 5c] due to the nickel oxidation in air.[49,51] It is well-known that the nickel is not stable in air and easily reacts with oxygen to form nickel oxide.[49,51] So, the CA is increased to 98°.

The CA value was measured after the droplets were dripped onto the samples for 5 s, and there was no scattering of contact angles along the surfaces. The average CA values were obtained by measuring the same samples at three different positions. From Figure 5c, one can see that the micro/nanocages can enhance hydrophobic ability of the nickel surface. The contact angles are 105.36°, 109.61°, 127.32°, and 142.16° for pulse energy of 0.05, 0.10, 0.15, and 0.20 mJ, respectively. It is obvious that the hydrophobicity greatly depends upon the heights and sizes of the micro/nanocages. The larger the micro/nanocages, the more the hydrophobicity. The schematic diagram for the hydrophobicity is illustrated in Figure 6a−d.

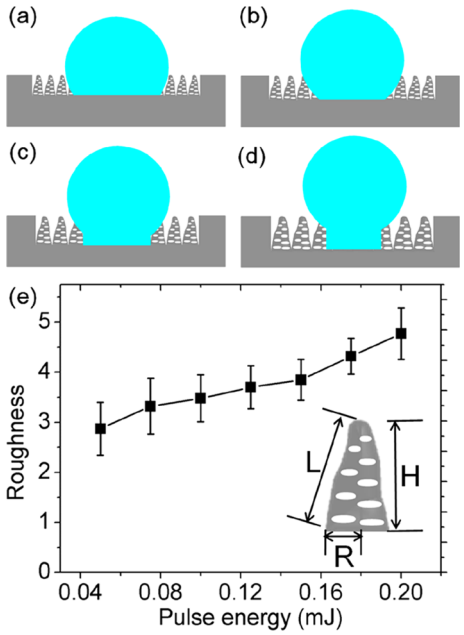

Figure 6. (a−d) The analysis of the wetting state between the water droplet and the samples, which are covered by various micro/nanocages under pulse energy of 0.05, 0.10, 0.15, and 0.20 mJ/pulse, respectively. (e) The roughness factors calculated from the data in Figure 4m. The biggest roughness factor can reach 4.77 for the microstructured nickel surfaces, which is much bigger than that of the flat surface ($f = 1$).

According to Wenzel's model,[48,52,53] the enhancement of hydrophobicity can be attributed to the increase of the roughness factor caused by the increasing heights of the micro/nanocages. In our case, micro/nanocage can be simplified as a cone, and the roughness factor can be expressed as

$$f = \frac{\pi \times R \times L}{\pi \times R^2} \quad (1)$$

where R is the radius of micro/nanocage bottom, which is equal to the size of the micro/nanocage. L is the generatrix of the micro/nanocage. On account of $L = (H^2 + R^2)^{1/2}$, the roughness factor formula can be rewritten as

$$f = \sqrt{1 + \left(\frac{H}{R}\right)^2} \quad (2)$$

where H is the height of the micro/nanocage. The roughness factor based on the data in Figure 4m is calculated, as shown in Figure 6e and Supporting Information, Tables S1 and S2. It is indicated that the roughness factor increased with the increasing micro/nanocage height. The biggest f can reach 4.77, which is much bigger than the one of flat surface ($f = 1$). In addition, the nanoholes (~100 nm) on the micro/nanocages also increase the superficial area of micro/nanocages, which further enhance the roughness factor. The maximum contact angle can reach as much as 142° without additional chemical modification. The contact angle may be over 160° if the surface is modified with low surface-energy materials.[52,53] The dust particles and any pollutants on the hydrophobic surface can be clearly washed by the water droplets[47,54] [Figure S5].

To investigate the durability of the micro/nanocages, we load the structures surface by a weight of 200 g and then scrub it slightly five times. The SEM results show that the micro/nanocages structures are well-preserved. In addtion, the water CA is 141.01°, almost no change compared with the previous one [Supporting Information, Figure S6].

CONCLUSION

In summary, large-area 3D porous metal micro/nanocages arrays are rapidly prepared on nickel surfaces by proposing a new method of one-step ethanol-assisted femtosecond laser irradiation. The formation process was in situ investigated by a series of femtosecond laser irradiation under exposure time from 5 to 30 ms, and its underlying mechanism is believed to be a combined process of accumulating pulse and confined plasmons. In addition, by tuning different laser energy from 0.05 to 0.2 mJ/pulse, the size of micro/nanocage arrays can be controlled from 0.8 to 1.9 μm. The 3D controllable cagelike micro/nanostructures exhibit not only enhanced antireflection from 80% to 7% but also hydrophobicity with CA from 98° to 142° without surface modification. We believe that this simple and rapid method for 3D large-area controllable metal micro/nanostructures may find broader applications in optoelectronics, industry, batteries, and chemical catalysis.

ASSOCIATED CONTENT

Supporting Information

Detailed fabrication of 3D metal arrays, irradiating nickel surface with pulse energy, 2D-FFT analysis, angle-dependent reflectance measurements, calculation of roughness factor, self-cleaning effect of micro/nanocages, durability of micro/nanocages. This material is available free of charge via the Internet at http://pubs.acs.org.

AUTHOR INFORMATION

Corresponding Authors

*E-mail: huyl@ustc.edu.cn. (Y.-L.H.)
*E-mail: dongwu@ustc.edu.cn. (D.W.)

Notes

The authors declare no competing financial interest.

■ ACKNOWLEDGMENTS

This work is supported by National Science Foundation of China (Nos. 51275502, 61475149, 51405464, 91223203, and 11204250), Anhui Provincial Natural Science Foundation (No. 1408085ME104), National Basic Research Program of China (No. 2011CB302100) and "Chinese Thousand Young Talents Program".

■ REFERENCES

(1) Pile, D. Photocatalysis: Plasmonic Enhancement. *Nat. Photonics* **2013**, *7*, 3−3.
(2) O'Brien, K.; Lanzillotti-Kimura, N. D.; Rho, J.; Suchowski, H.; Yin, X.; Zhang, X. Ultrafast Acousto-plasmonic Control and Sensing in Complex Nanostructures. *Nat. Commun.*. **2014**, *5*.
(3) Piglosiewicz, B.; Schmidt, S.; Park, D. J.; Vogelsang, J.; Groß, P.; Manzoni, C.; Farinello, P.; Cerullo, G.; Lienau, C. Carrier-envelope Phase Effects on the Strong-field Photoemission of Electrons from Metallic Nanostructures. *Nat. Photonics* **2014**, *8*, 37−42.
(4) Shoji, T.; Saitoh, J.; Kitamura, N.; Nagasawa, F.; Murakoshi, K.; Yamauchi, H.; Ito, S.; Miyasaka, H.; Ishihara, H.; Tsuboi, Y. Permanent Fixing or Reversible Trapping and Release of DNA Micropatterns on a Gold Nanostructure Using Continuous-wave or Femtosecond-pulsed Near-infrared Laser Light. *J. Am. Chem. Soc.* **2013**, *135*, 6643−6648.
(5) Linic, S.; Christopher, P.; Ingram, D. B. Plasmonic-metal Nanostructures for Efficient Conversion of Solar to Chemical Energy. *Nat. Mater.* **2011**, *10*, 911−921.
(6) Valsecchi, C.; Brolo, A. G. Periodic Metallic Nanostructures as Plasmonic Chemical Sensors. *Langmuir* **2013**, *29*, 5638−5649.
(7) Near, R.; Tabor, C.; Duan, J.; Pachter, R.; El-Sayed, M. Pronounced Effects of Anisotropy on Plasmonic Properties of Nanorings Fabricated by Electron Beam Lithography. *Nano Lett.* **2012**, *12*, 2158−2164.
(8) Lin, Y. Y.; Liao, J. D.; Ju, Y. H.; Chang, C. W.; Shiau, A. L. Focused Ion Beam-fabricated Au Micro/nanostructures Used as a Surface Enhanced Raman Scattering-active Substrate for Trace Detection of Molecules and Influenza Virus. *Nanotechnology* **2011**, *22*, 185308.
(9) Pilet, N.; Raabe, J.; Stevenson, S. E.; Romer, S.; Bernard, L.; McNeill, C. R.; Fink, R. H.; Hug, H. J.; Quitmann, C. Nanostructure Characterization by a Combined X-ray Absorption/Scanning Force Microscopy System. *Nanotechnology* **2012**, *23*, 475708.
(10) Ye, X. Z.; Qi, L. M. Two-dimensionally Patterned Nanostructures Based on Monolayer Colloidal Crystals: Controllable Fabrication, Assembly, and Applications. *Nano Today* **2011**, *6*, 608−631.
(11) Chang, C. H.; Tian, L.; Hesse, W. R.; Gao, H.; Choi, H. J.; Kim, J. G.; Siddiqui, M.; Barbastathis, G. From Two-dimensional Colloidal Self-Assembly to Three-Dimensional Nanolithography. *Nano Lett.* **2011**, *11*, 2533−2537.
(12) Tsuyoshi, T. Metal-Vapor Deposition Modulation on Polymer Surfaces Prepared by the Coffee-Ring Effect. *Soft Matter* **2013**, *9*, 5681−5685.
(13) Gecys, P.; Markauskas, E.; Gedvilas, M.; Raciukaitis, G.; Repins, I.; Beall, C. Ultrashort Pulsed Laser Induced Material Lift-Off Processing of CZTSe Thin-film Solar Cells. *Sol. Energy* **2014**, *102*, 82−90.
(14) Masui, K.; Shoji, S.; Asaba, K.; Rodgers, T. C.; Jin, F.; Duan, X. M.; Kawata, S. Laser Fabrication of Au Nanorod Aggregates Microstructures Assisted by Two-photon Polymerization. *Opt. Express* **2011**, *19*, 22786−22796.
(15) Vora, K.; Kang, S. Y.; Shukla, S.; Mazur, E. Fabrication of Disconnected Three-dimensional Silver Nanostructures in a Polymer Matrix. *Appl. Phys. Lett.* **2012**, *100*, 063120.
(16) Wang, J. C.; Guo, C. L. Ultrafast Dynamics of Femtosecond Laser-induced Periodic Surface Pattern Formation on Metals. *Appl. Phys. Lett.* **2005**, *87*, 251914.
(17) Sakabe, S.; Hashida, M.; Tokita, S.; Namba, S.; Okamuro, K. Mechanism for Self-formation of Periodic Grating Structures on a Metal Surface by a Femtosecond Laser Pulse. *Phys. Rev. B* **2009**, *79*, 033409.
(18) Nayak, B. K.; Gupta, M. C.; Kolasinski, K. W. Formation of Nano-textured Conical Microstructures in Titanium Metal Surface by Femtosecond Laser Irradiation. *Appl. Phys. A: Mater. Sci. Process.* **2008**, *90*, 399−402.
(19) Kuznetsov, A. I.; Kiyan, R.; Chichkov, B. N. Laser fabrication of 2D and 3D Metal Nanoparticle Structures and Arrays. *Opt. Express* **2010**, *18*, 21198−21203.
(20) Vorobyev, A. Y.; Guo, C. L. Colorizing Metals with Femtosecond Laser Pulses. *Appl. Phys. Lett.* **2008**, *92*, 041914.
(21) Li, G. Q.; Li, J. W.; Yang, L.; Li, X. H.; Hu, Y. L.; Chu, J. R.; Huang, W. H. Evolution of Aluminum Surface Irradiated by Femtosecond Laser Pulses with Different Pulse Overlaps. *Appl. Surf. Sci.* **2013**, *276*, 203−209.
(22) Dusser, B.; Sagan, Z.; Soder, H.; Faure, N.; Colombier, J. P.; Jourlin, M.; Audouard, E. Controlled Nanostructrures Formation by Ultra Fast Laser Pulses for Color Marking. *Opt. Express* **2010**, *18*, 2913−2924.
(23) Ou, Z. G.; Huang, M.; Zhao, F. L. Colorizing Pure Copper Surface by Ultrafast Laser-induced Near-Subwavelength Ripples. *Opt. Express* **2014**, *22*, 17254−17265.
(24) Yao, J. W.; Zhang, C. Y.; Liu, H. Y.; Dai, Q. F.; Wu, L. J.; Lan, S.; Gopal, A. V.; Trofimov, V. A.; Lysak, T. M. Selective Appearance of Several Laser-induced Periodic Surface Structure Patterns on a Metal Surface Using Structural Colors Produced by Femtosecond Laser Pulses. *Appl. Surf. Sci.* **2012**, *258*, 7625−7632.
(25) Anyfantis, G. C.; Papavassiliou, G. C.; Assimomytis, N.; Terzis, A.; Psycharis, V.; Raptopoulou, C. P.; Kyritsisc, P.; Thoma, V.; Koutselas, I. B. Some Unsymmetrical Nickel 1, 2-dithiolene Complexes as Candidate Materials for Optics and Electronics. *Solid State Sci.* **2008**, *10*, 1729−1733.
(26) Lenhart, S. J.; Macdonald, D. D.; Pound, B. G. An AC Impedance Study of the Degradation of Porous Nickel Battery Electrodes. *J. Electrochem. Soc.* **1988**, *135*, 1063−1071.
(27) Roy, S.; Majhi, T.; Kundu, A.; Sarkar, C. K.; Saha, H. Design, Fabrication and Simulation of Coplanar Microheater Using Nickel Alloy for Low Temperature Gas Sensing Application. *Sens. Lett.* **2011**, *9*, 1382−1389.
(28) Sergeev, A. G.; Hartwig, J. F. Selective, Nickel-catalyzed Hydrogenolysis of Aryl Ethers. *Science* **2011**, *332*, 439−443.
(29) Han, Z. J.; Qiu, F.; Eisenberg, R.; Holland, P. L.; Krauss, T. D. Robust Photogeneration of H_2 in Water Using Semiconductor Nanocrystals and a Nickel Catalyst. *Science* **2012**, *338*, 1321−1324.
(30) Tang, Y. F.; Yang, J. J.; Zhao, B.; Wang, M. W.; Zhu, X. N. Control of Periodic Ripples Growth on Metals by Femtosecond Laser Ellipticity. *Opt. Express* **2012**, *20*, 25826−25833.
(31) Yang, Y.; Yang, J. J.; Xue, L.; Guo, Y. Surface Patterning on Periodicity of Femtosecond Laser-induced Ripples. *Appl. Phys. Lett.* **2010**, *97*, 141101.
(32) Zuhlke, C. A.; Anderson, T. P.; Alexander, D. R. Comparison of the Structural and Chemical Composition of Two Unique Micro/nanostructures Produced by Femtosecond Laser Interactions on Nickel. *Appl. Phys. Lett.* **2013**, *103*, 121603.
(33) Zuhlke, C. A.; Anderson, T. P.; Alexander, D. R. Formation of Multiscale Surface Structures on Nickel via Above Surface Growth and Below Surface Growth Mechanisms Using Femtosecond Laser Pulses. *Opt. Express* **2013**, *21*, 8460.
(34) Hwang, T. Y.; Vorobyev, A. Y.; Guo, C. L. Formation of Solar Absorber Surface on Nickel with Femtosecond Laser Irradiation. *Appl. Phys. A: Mater. Sci. Process.* **2012**, *108*, 299.
(35) Yang, G. W. Laser Ablation in Liquids: Applications in the Synthesis of Nanocrystals. *Prog. Mater. Sci.* **2007**, *52*, 648−698.
(36) Shaheen, M. E.; Gagnon, J. E.; Fryer, B. J. Femtosecond Laser Ablation of Brass in Air and Liquid Media. *J. Appl. Phys.* **2013**, *113*, 213106.
(37) Barmina, E. V.; Stratakis, E.; Barberoglou, M.; Stolyarov, V. N.; Stolyarov, I. N.; Fotakis, C.; Shafeev, G. A. Laser-assisted Nano-

structuring of Tungsten in Liquid Environment. *Appl. Surf. Sci.* **2012**, *258*, 5898−5902.
(38) Bashira, S.; Rafiquea, M. S.; Nathala, C. S.; Husinsky, W. The Formation of Nanodimensional Structures on the Surface of Tin Exposed to Femtosecond Laser Pulses in the Ambient Environment of Ethanol. *Appl. Surf. Sci.* **2014**, *290*, 53−58.
(39) Albu, C.; Dinescu, A.; Filipescu, M.; Ulmeanu, M.; Zamfirescu, M. Periodical Structures Induced by Femtosecond Laser on Metals in Air and Liquid Environments. *Appl. Surf. Sci.* **2013**, *278*, 347−351.
(40) Lungu, C. P.; Ticos, C. M.; Poroşnicu, C.; Jepu, I.; Lungu, M.; Marcu, A.; Luculescu, C.; Cojocaru, G.; Ursescu, D.; Banici, R.; Ungureanu, G. R. Periodic Striations on Beryllium and Tungsten Surfaces by Indirect Femtosecond Laser Irradiation. *Appl. Phys. Lett.* **2014**, *104*, 101604.
(41) Harzic, R. L.; Dörr, D.; Sauer, D.; Stracke, F.; Zimmermann, H. Generation of High Spatial Frequency Ripples on Silicon under Ultrashort Laser Pulses Irradiation. *Appl. Phys. Lett.* **2011**, *98*, 211905.
(42) Søndergaard, T.; Novikov, S. M.; Holmgaard, T.; Eriksen, R. L.; Beermann, J.; Han, Z.; Pedersen, K.; Bozhevolnyi, S. I. Plasmonic Black Gold by Adiabatic Nanofocusing and Absorption of Light in Ultra-sharp Convex Grooves. *Nat. Commun.* **2012**, *3*, 969.
(43) Vorobyev, A. Y.; Topkov, A. N.; Gurin, O. V.; Svich, V. A.; Guo, C. L. Enhanced Absorption of Metals over Ultrabroad Electromagnetic Spectrum. *Appl. Phys. Lett.* **2009**, *95*, 121106.
(44) Vorobyev, A. Y.; Makin, V. S.; Guo, C. L. Brighter Light Sources from Black Metal: Significant Increase in Emission Efficiency of Incandescent Light Sources. *Phys. Rev. Lett.* **2009**, *102*, 234301.
(45) Vorobyev, A. Y.; Guo, C. L. Direct Creation of Black Silicon Using Femtosecond Laser Pulses. *Appl. Surf. Sci.* **2011**, *257*, 7291−7294.
(46) Jiang, H. B.; Zhang, Y. L.; Han, D. D.; Xia, H.; Feng, J.; Chen, Q. D.; Hong, Z. R.; Sun, H. B. Biomimetics: Bioinspired Fabrication of Superhydrophobic Graphene Films by Two-beam Laser Interference. *Adv. Funct. Mater.* **2014**, *24*, 4720−4720.
(47) Wu, D.; Wu, S. Z.; Chen, Q. D.; Zhang, Y. L.; Yao, J.; Yao, X.; Niu, L. G.; Wang, J. N.; Jiang, L.; Sun, H. B. Curvature-driven Reversible in Situ Switching Between Pinned and Roll-Down Superhydrophobic States for Water Droplet Transportation. *Adv. Mater.* **2011**, *23*, 545−549.
(48) Yong, J. L.; Chen, F.; Yang, Q.; Zhang, D. S.; Bian, H.; Du, G. Q.; Si, J. H.; Meng, X. W.; Hou, X. Controllable Adhesive Superhydrophobic Surfaces Based on PDMS Microwell Arrays. *Langmuir* **2013**, *29*, 3274−3279.
(49) Khorsand, S.; Raeissi, K.; Ashrafizadeh, F. Corrosion Resistance and Long-term Durability of Super-hydrophobic Nickel Film Prepared by Electrodeposition Process. *Appl. Surf. Sci.* **2014**, *305*, 498−505.
(50) Li, G. Y.; Li, X. P.; Wang, H.; Yang, Z. Q.; Yao, J. Y.; Ding, G. F. Fabrication and Characterization of Superhydrophobic Surface by Electroplating Regular Rough Micro-structures of Metal Nickel. *Microelectron. Eng.* **2012**, *95*, 130−135.
(51) Boinovich, L. B.; Emelyanenko, A. M.; Pashinin, A. S.; Lee, C. H.; Drelich, J.; Yap, Y. K. Origins of Thermodynamically Stable Superhydrophobicity of Boron Nitride Nanotubes Coatings. *Langmuir* **2012**, *28*, 1206−1216.
(52) Wu, D.; Chen, Q. D.; Xia, H.; Jiao, J.; Xu, B. B.; Lin, X. F.; Xu, Y.; Sun, H. B. A Facile Approach for Artificial Biomimetic Surfaces with Both Superhydrophobicity and Iridescence. *Soft Matter* **2010**, *6*, 263.
(53) Chen, F.; Zhang, D. S.; Yang, Q.; Yong, J. L.; Du, G. Q.; Si, J. H.; Yun, F.; Hou, X. Bioinspired Wetting Surface via Laser Microfabrication. *ACS Appl. Mater. Interfaces* **2013**, *5*, 6777−6792.
(54) Blossey, R. Self-cleaning Surfaces-virtual Realities. *Nat. Mater.* **2003**, *2*, 301−306.